Twist, tilt, and orientational order at the nematic to twist-bend nematic phase transition of 1″,9″-bis(4-cyanobiphenyl-4′-yl) nonane: A dielectric, ^{2}H NMR, and calorimetric study

Beatriz Robles-Hernández,[1] Nerea Sebastián,[1,2] M. Rosario de la Fuente,[1,*] David O. López,[3] Sergio Diez-Berart,[3] Josep Salud,[3] M. Blanca Ros,[4] David A. Dunmur,[5,†] Geoffrey R. Luckhurst,[5] and Bakir A. Timimi[5]

[1]*Departamento de Física Aplicada II, Facultad de Ciencia y Tecnología, Universidad del País Vasco, Apartado 644, E-48080 Bilbao, Spain*

[2]*Otto-von-Guericke Universitat Magdeburg, Institute for Experimental Physics, ANP, 39106 Magdeburg, Germany*

[3]*Grup de Propietas Físiques dels Materials (GRPFM), Departament de Física i Enginyeria Nuclear, E.T.S.E.I.B. Universitat Politècnica de Catalunya, Diagonal 647, E- 08028 Barcelona, Spain*

[4]*Departamento de Química Orgánica, Facultad de Ciencias–Instituto de Ciencia de Materiales de Aragón, Universidad de Zaragoza-CSIC, E-50009 Zaragoza, Spain*

[5]*Chemistry, University of Southampton, Highfield, Southampton SO17 1BJ, United Kingdom*

(Received 6 October 2015; published 2 December 2015)

The nature of the nematic-nematic phase transition in the liquid crystal dimer 1″,9″-bis(4-cyanobiphenyl-4′-yl) nonane (CB9CB) has been investigated using techniques of calorimetry, dynamic dielectric response measurements, and ^{2}H NMR spectroscopy. The experimental results for CB9CB show that, like the shorter homologue CB7CB, the studied material exhibits a normal nematic phase, which on cooling undergoes a transition to the twist-bend nematic phase (N_{TB}), a uniaxial nematic phase, promoted by the average bent molecular shape, in which the director tilts and precesses describing a conical helix. Modulated differential scanning calorimetry has been used to analyze the nature of the N_{TB}-N phase transition, which is found to be weakly first order, but close to tricritical. Additionally broadband dielectric spectroscopy and ^{2}H magnetic resonance studies have revealed information on the structural characteristics of the recently discovered twist-bend nematic phase. Analysis of the dynamic dielectric response in both nematic phases has provided an estimate of the conical angle of the heliconical structure for the N_{TB} phase. Capacitance measurements of the electric-field realignment of the director in initially planar aligned cells have yielded values for the splay and bend elastic constants in the high temperature nematic phase. The bend elastic constant is small and decreases with decreasing temperature as the twist-bend phase is approached. This behavior is expected theoretically and has been observed in materials that form the twist-bend nematic phase. ^{2}H NMR measurements characterize the chiral helical twist identified in the twist-bend nematic phase and also allow the determination of the temperature dependence of the conical angle and the orientational order parameter with respect to the director.

DOI: 10.1103/PhysRevE.92.062505 PACS number(s): 61.30.Eb, 64.70.mj

I. INTRODUCTION

During the last few years interest in liquid crystal dimers has experienced an extraordinary growth due to the observation of nematic-nematic transitions for relatively simple materials where two mesogenic units are linked by methylene chains having odd numbers of carbon atoms [1–5]. Although the high temperature nematic mesophase of these materials is a conventional nematic phase, its elastic and dielectric properties are far from typical [2,6–8]. In contrast to normal low molecular weight nematic liquid crystals, odd dimers possess a bend elastic constant (K_3) significantly smaller than the splay elastic constant (K_1) [6,9,10]. Moreover, K_3 reduces with decreasing temperature reaching remarkably low values [7,9,10]. Such behavior has been successfully explained in terms of the effect the molecular shape exerts on elastic constants [11], the preferred averaged bent molecular shape promoted by the odd spacers being responsible for the low or possibly negative bend elastic constants [12]. This is especially the case when the spacer is linked by methylene groups to the mesogenic groups [13]. According to Dozov's predictions [12], a negative bend elastic coefficient [14] would give rise to a nematic ground state where the director, instead of being uniformly aligned, spontaneously bends. This state of bend deformation would have to be accompanied by a splay or twist deformation in order to be stabilized. In the latter case, the induced twist could be left- or right-handed, and thus, even though molecules are achiral, the sample would be expected to form a conglomerate of domains having opposite chirality, that is, a nematic phase where the directors arrange themselves into a helix with the director making a constant angle with respect to it [12]. Recently we have reported [15] a twist-bend nematic (N_{TB}) mesophase for ether-linked dimers formed at low temperatures from the nematic-isotropic transition: Other authors have also claimed to have observed the twist-bend nematic phase with ether-linked dimers, but no results to support this claim are given in their paper [16].

Following a detailed investigation of the liquid crystal dimer 1″,7″-bis(4-cyanobiphenyl-4′-yl) heptane (CB7CB) [2] it was proposed that the low temperature nematic phase observed for such odd dimers is indeed the N_{TB} phase predicted by Dozov [12]. This study has been followed by intense research activity focused on the structure and properties of the N_{TB} phase. Different authors have described a characteristic ropelike texture with stripes parallel to the alignment axis for thin films of planar aligned samples [1,2,9,16,17]. With the sample between a cover slip and microscope slide, focal-conic-defect and parabolic-defect textures have been

*rosario.delafuente@ehu.es
†d.dunmur@tiscali.co.uk

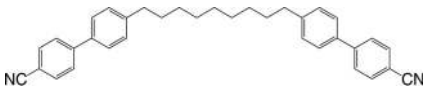

FIG. 1. Chemical structure of the methylene-linked dimer 1″,9″-bis(4-cyanobiphenyl-4′-yl) nonane (CB9CB).

observed [2,16], both indicative of a periodic modulation of the refractive indices. However, the possibility of smecticlike order was initially excluded by careful x-ray experiments, which showed no Bragg reflections [2,4,7,9]. This observation rules out long-range translational order in the phase, but does not exclude the possibility of other structural order characterized by appropriate order parameters. Through ^{2}H NMR investigations, the chiral character of this nematic phase has been unambiguously confirmed in agreement with Dozov's predictions [18–21]. Recently, nanoscale helix pitch periodicities of 8−10 nm have been measured in the N_{TB} phase using freeze fracture transmission electron microscopy (FFTEM), and similar values have been obtained from a theoretical analysis of quadrupolar splittings measured for 8CB-d_2 dissolved in CB7CB [7,21,22]. Interestingly, although composed of nonchiral molecules, electroclinic effects typical of chiral systems have been also reported [23–25]. Broadband dielectric studies of this compound [2,8] show that both nematic mesophases have a very similar dielectric behavior. An interesting question concerns the character or the N_{TB}-N phase transition. Although some theoretical approaches [12,26] seem to predict a second-order phase transition, calorimetric results point to a first-order phase transition although with a strength that changes with the molecular structure, such as the spacer length [2,8].

The current paper focuses on the liquid crystal dimer 1″,9″-bis(4-cyanobiphenyl-4′-yl) nonane (hereafter referred to as CB9CB; see Fig. 1) that belongs to the same homologous series of methylene-linked cyanobiphenyl-alkane dimers as the first reported [2] example of a twist-bend nematic phase, CB7CB. High-resolution adiabatic scanning calorimetry measurements, miscibility studies, and x-ray investigations of CB9CB by Tripathi *et al.* [4] have demonstrated that, similar to its shorter-chain homologue CB7CB, CB9CB exhibits two nematic phases. However, in that study no mention is made concerning the nature of the low temperature nematic phase. In this paper we present a comprehensive experimental study of both nematic phases of CB9CB that allows us to identify the low temperature nematic phase as a twist-bend nematic phase. The static dielectric permittivity measurements presented here constitute direct evidence of changes in the conformational distribution in the mesophases, while studies of the dynamics of the dipolar groups at the N-N_{TB} transition provide clear proof of the tilt of the director in the lower temperature mesophase. Since it has been proposed that elastic constants contribute to the stability of the N_{TB} phase [12], K_1 and K_3 have been determined using Fréedericksz-transition experiments. The chiral structure associated with the heliconical twist-bend nematic phase is established by ^{2}H NMR experiments using CB7CB-d_4 as a spin probe which allows a measure of the phase chirality to be established, together with the orientational order and the director tilt. Additionally, by means of high-resolution calorimetry experiments we present a detailed description of the N-I and N_{TB}-N phase transitions. Finally, our study reveals the existence of a glassy state linked to the twist-bend nematic phase.

The layout of the paper is as follows. In Sec. II we describe the experimental details. In Sec. III we present and discuss our results concerning the heat capacity data, optical microscopy, dielectric permittivity, splay and bend elastic constants, and the quadrupolar splittings from ^{2}H NMR spectroscopy. Our concluding remarks are summarized in Sec. IV.

II. EXPERIMENTAL DETAILS

A. Material

The symmetric liquid crystal dimer CB9CB was synthesized using the methodology previously reported for CB7CB [13]. The liquid crystalline behavior was characterized using its optical textures and modulated differential scanning calorimetry (MDSC). The phase sequence obtained (as detailed in Sec. III A) is in good agreement with earlier studies that noted a nematic-nematic phase transition in CB9CB [4], but did not identify the low-temperature phase or give any indications of its structure. Recently, Hoffmann *et al.* [27] have used ^{2}H NMR to study CB9CB and found that the deuterium quadrupolar tensor in the twist-bend nematic phase was uniaxial which is in accord with the global symmetry of the phase. Their results are consistent with earlier measurements made on CB7CB-d_4 [2]. Hoffmann *et al.* [27] argue that the lack of local biaxiality shows that the phase does not have the structure proposed for the twist-bend nematic. However, it has been pointed out [28] that sufficiently rapid translational diffusion along the helix axis will average out the local biaxiality, as happens with conventional chiral nematic phases. Proton NMR measurements have indeed shown that translational diffusion parallel to the helix axis is fast enough to remove the biaxiality of the quadrupolar tensor, which as a result appears to be uniaxial [28].

The ^{2}H NMR studies were performed on a sample of the dimer CB9CB doped with 2 wt% of CB7CB-d_4 [2]. This particular spin probe was chosen as the deuterium source because of its structural similarity to the host, CB9CB; the transition temperatures of CB7CB are just a few degrees lower than those of CB9CB; as a result the transition temperatures of the doped samples are depressed by about 1 K by the addition of the probe.

B. Experimental techniques

Heat capacity measurements at atmospheric pressure were made using a commercial differential scanning calorimeter DSC-Q2000 from TA Instruments working in the modulated mode (MDSC). Like an alternating current (ac) calorimeter, the MDSC technique, besides providing heat capacity data, simultaneously gives phase shift data that allow the determination of the two-phase coexistence region for weakly first-order phase transitions. In our work, experimental conditions were adjusted in such a way that the imaginary part of the complex heat capacity data vanished. The MDSC technique is also suitable for quantitative measurements of latent heats for first-order transitions, even if they are weak. A more detailed description of the MDSC technique can be found elsewhere [29].

The MDSC measurements were made following different procedures. For a standard study of the overall thermal behavior of the sample, heating runs at 1 K min^{-1} from room temperature up to the isotropic phase and cooling runs at several cooling rates were performed. Additionally, in order to study the nature of the N_{TB}-N and N-I phase transitions, high-resolution heating and cooling runs at a rate of 0.01 K min^{-1} were performed in a temperature interval of about 5 K around the transition. Modulation parameters (temperature amplitude and oscillation period) were ±0.5 K and 60 s in the standard mode and ±0.07 K and 23 s in the high-resolution mode. Sample masses (between 2 and 3 mg) were selected to ensure a uniform thin layer within the aluminum pans.

Static dielectric permittivity measurements at 5 kHz were performed on an Instec cell of 8 μm thickness with antiparallel planar rubbing and a pretilt of between 1° and 3° (specified by Instec). The empty cell capacity was carefully calibrated before filling, and sealed afterward to prevent bubble formation. The experiment includes an Agilent Precision LRC meter E4890A that allows for the application of ac fields from 20 Hz to 2 MHz with probe voltages up to 20 V_{rms}. Samples were held on a hot stage (TMSG-600) with a temperature controller (TMS-93), both from Linkam. The hot stage was placed on a polarizing microscope (BH2 Olympus) equipped with a camera (Olympus C5050) for the observation and recording of optical textures. This setup was also employed for the measurement of the splay and bend elastic constants from the voltage dependence of the capacitance of the sample through the Fréedericksz transition. The electric-field strength was varied from 0.1 to 16 V_{rms}, with a waiting time of 30 s between the application of the field and the acquisition of the capacitance value to guarantee the achievement of the equilibrium director distribution. Details of the data analysis are given in Sec. III B 1.

The complex dielectric permittivity $\varepsilon^*(\omega) = \varepsilon'(\omega) - i\varepsilon''(\omega)$ was measured over the frequency range $10^3 - 1.8 \times 10^9$ Hz by combining two impedance analyzers: HP4192A and HP4291A. High-frequency dielectric measurements require the utilization of cells with untreated metal electrodes. In our setup the cell consists of a parallel plate capacitor made of two circular gold-plated brass electrodes 5 mm in diameter separated by 50-μm-thick silica spacers. It was placed at the end of a coaxial line and a modified HP16091A coaxial test fixture was used as the sample holder and then held in a Novocontrol cryostat, which screens the system. Dielectric measurements were performed on cooling with different temperature steps being stabilized to ±20 mK.

The ^{2}H NMR spectra were measured on a Varian Chemagnetics CMX Infinity spectrometer which has a magnetic field strength of 9.40 T. In the nematic phase the director is aligned parallel to the field and in the twist-bend nematic it is the helix axis that aligns parallel to the magnetic field [18]. The sample was placed in a short NMR tube 5 mm in diameter and the tube was arranged orthogonal to the magnetic field. The sample temperature is controlled by a Chemagnetics temperature controller; it is stable to ±0.3 K during the spectral measurements and the transition temperatures of the doped mesogen were used to calibrate the controller to about ±0.5 K. The spectra were measured using a single pulse sequence with a pulse width of 5 μs. The relaxation delay between the end of the acquisition of the free induction decay, FID and the pulse was set at 0.05 s. Typically 10000 FIDs were acquired into 4096 words of computer memory with a spectral window of 250 kHz.

III. RESULTS AND DISCUSSION

A. Mesophase behavior and calorimetry

The phase sequence of CB9CB was studied in the past by means of high-resolution adiabatic calorimetry and conventional DSC [4] revealing only two mesophases. By means of x-ray investigations the high temperature phase was identified as a conventional uniaxial nematic phase, and a second unidentified nematic phase appeared at lower temperatures [4]. Our studies of CB9CB show that on cooling from the isotropic phase, a nematic phase is formed at about 394 K, as can be clearly identified from the characteristic uniform nematic texture obtained in planar cells, and the Schlieren texture formed in cells with no alignment treatment. Further cooling reveals another mesophase, which propagates along the cell leading to an initial quasiuniform texture [see Fig. 2(a)] that develops systematically into a striped texture [see Fig. 2(b)]. The stripes grow slowly parallel to the surface easy axis with a periodicity of the order of twice the cell thickness as reported for other twist-bend nematic forming dimers [1,17]. For slow cooling rates, the stripes are totally developed showing tilted bands across them, as in a ropelike texture, characteristic of a

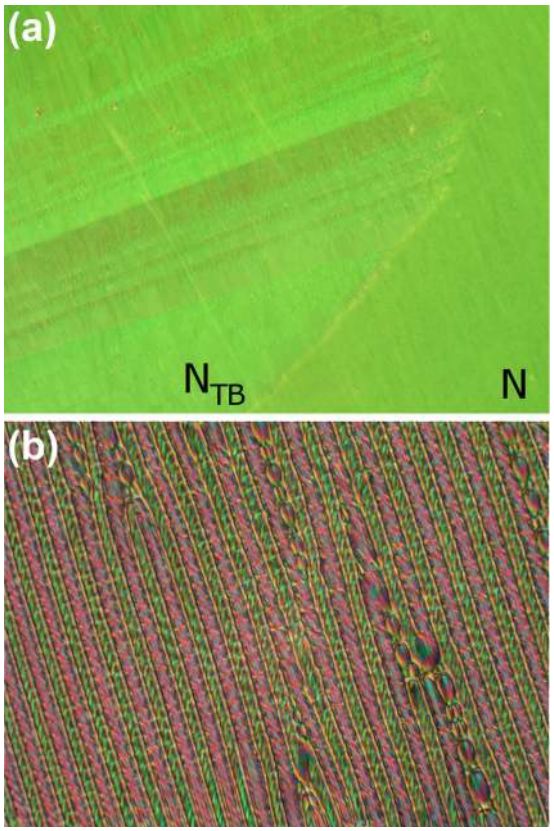

FIG. 2. (Color online) Optical textures obtained in 8-μm-thick cells (antiparallel alignment, from Instec). (a) At the N_{TB}-N transition; width of the microphotograph 575 μm. (b) Ropelike texture; width of the microphotograph 300 μm.

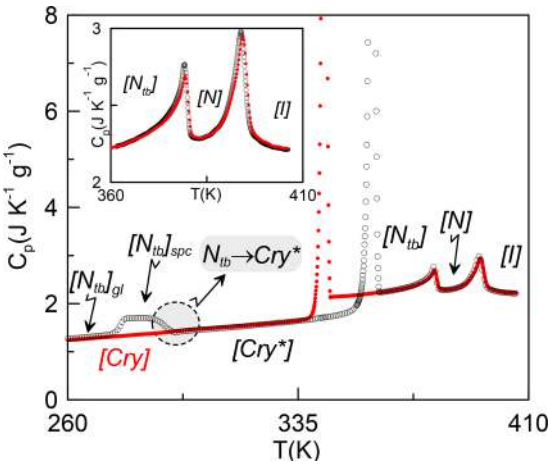

FIG. 3. (Color online) Heat capacity data as a function of temperature on heating at 1 K min^{-1} after cooling the sample from the I phase at 30 K min^{-1} (open symbols) and 1 K min^{-1} (full symbols). Inset shows a zoom on the N_{TB}-N and N-I transitions for both conditions.

twist-bend nematic phase [2], while for faster cooling rates a less uniform texture with regions of focal conics is observed. When rotating the sample with respect to the crossed polarizers bright and dark states are revealed which suggest that there are optical extinction positions that make an angle with the axis of the stripes.

Measurements of the heat capacity as a function of temperature over a wide temperature range are given in Fig. 3. Black and red symbols correspond to data recorded on heating at 1 K min^{-1} from 260 K with the sample in two different states: after cooling the sample from the isotropic phase at 30 K min^{-1} (black symbols) and after slow cooling at 1 K min^{-1} (red symbols). The fast cooling rate of 30 K min^{-1} is sufficiently high to prevent crystallization and the twist-bend nematic phase becomes a glassy state ($[N_{\mathrm{TB}}]_{gl}$). It should be stressed that for slower cooling rates (for example, 20 K min^{-1}), the sample partially crystallizes giving rise to a coexistence of a crystalline state with a glassy state. Figure 3 clearly shows the characteristic heat capacity jump assigned to the glass transition and how the sample in the supercooled N_{TB} phase crystallizes irreversibly on heating at about 285 K (black symbols). The crystalline state obtained in this way has the same heat capacity value as the crystalline state obtained by slow cooling (red symbols) but both crystalline states are clearly different as can be inferred from the separation of about 15 K of their melting points. Irrespective of the initial crystalline state, once the phase transition to the lower temperature nematic phase takes place, both the N_{TB}-N and the N-I phase transitions are observed to be identical as is shown in the inset of Fig. 3. The characteristic temperatures corresponding to the different phase transitions are listed in Table I.

The MDSC technique through the heat capacity data allows us to obtain the latent heat associated with the first-order phase transitions. The total enthalpy change associated with any transition (ΔH^{TOT}) can be written as

$$\Delta H^{\mathrm{TOT}} = \Delta H + \int \Delta C_p dT, \tag{1}$$

where the second term on the right-hand side of Eq. (1) is the pretransitional fluctuation contribution (ΔC_p being the difference $C_p - C_{p,\mathrm{background}}$ due to the change in the orientational order intrinsic to this transition) and ΔH is the latent heat which vanishes for second-order transitions. In strongly first-order phase transitions, the second term of the right-hand side of Eq. (1) can be neglected and the total enthalpy change is identified with the latent heat associated with the phase transition. This applies to the latent heat obtained for the Cry-N_{TB} transition (considering the crystal phase formed by slow cooling), and the result is listed in Table I. The results are in quite good agreement with the value reported by Tripathi *et al.* [4]. The latent heat associated with the N-I and N_{TB}-N phase transitions deserves a special mention and will be analyzed in the following sections: Secs. III A 1 and III A 2.

1. *The N-I phase transition*

The theoretical description of the uniaxial N-I phase transition through the Landau–de Gennes theory is similar to the mean-field Landau model, but in the free energy density expansion of the nematic phase in terms of the scalar order parameter Q_N, identified with the average value of the second Legendre polynomial $\langle P_2(\cos\theta_i)\rangle$ with θ_i the angle of the ith molecule with respect to the nematic director, a cubic term B is needed:

$$F_N = F_I + AQ_N^2 + BQ_N^3 + CQ_N^4 + DQ_N^6 + \cdots. \tag{2}$$

The B parameter is the so-called cubic invariant and is responsible for the first-order character of the N-I phase transition. If B is very small and the other parameters A and C become simultaneously zero, the N-I phase transition

TABLE I. Transition temperatures ($T_{\mathrm{Cry}N_{\mathrm{TB}}}$, T_g, $T_{N_{\mathrm{TB}}N}$, and T_{NI}) and transition entropies ($\Delta S_{\mathrm{Cry}N_{\mathrm{TB}}}/R$, $\Delta S_{N_{\mathrm{TB}}N}/R$, and $\Delta S_{NI}/R$).

$T_{\mathrm{Cry}N_{\mathrm{TB}}}$ (K)	$\Delta S_{\mathrm{Cry}N_{\mathrm{TB}}}/R$	T_g (K)	$T_{N_{\mathrm{TB}}N}$ (K)	$\Delta S_{N_{\mathrm{TB}}N}/R$	T_{NI} (K)	$\Delta S_{NI}/R$	Reference
–	–	–	377.22	0.037 ± 0.002	392.92	0.18 ± 0.02	Ref. [4][a]
			380.45	–	395.90	–	Ref. [4][b]
357.6[c]	10.6[c]	277.2[d]	379.09	0.038 ± 0.006[e]	394.92	0.16 ± 0.02[e]	This work

[a]Data from adiabatic scanning calorimetry (ASC) at 0.15 K h^{-1}.
[b]Data from DSC traces.
[c]From MDSC data on heating at 1 K min^{-1}. The sample was previously cooled at 1 K min^{-1}.
[d]From MDSC data on heating at 1 K min^{-1}. The sample was previously cooled at 20 K min^{-1}.
[e]From MDSC data on heating at 0.01 K min^{-1}.

becomes strictly tricritical [30,31]. In such a situation the heat capacity critical exponent α in both the N and I phases must be $\frac{1}{2}$ and the Q_N critical exponent β must be $\frac{1}{4}$. From an experimental point of view, such parameters can be obtained from very accurate heat capacity data through the N-I phase transition.

Figure 4 shows the heat capacity together with the ϕ-phase shift data around the N-I phase transition. The sharp peak in ϕ-phase shift data at the transition temperature is a signature of the first-order character of the N-I phase transition and will be used to delimit the coexistence region by the dashed lines in Fig. 4.

The critical behavior of the heat capacity around the N-I phase transition follows the standard expressions [15,30,32,33] in a region of no more than ± 3 K around T_{NI}:

$$C_{p,I} = B_C + D_C\left[\frac{T}{T^*} - 1\right] + A_{C,I}\left|\frac{T}{T^*} - 1\right|^{-\alpha}, \quad \text{for } T > T_{NI} = T^* + \Delta T^*, \tag{3a}$$

$$C_{p,N} = B_C + D_C\left[\frac{T}{T^{**}} - 1\right] + A_{C,N}\left|\frac{T}{T^{**}} - 1\right|^{-\alpha}, \quad \text{for } T < T_{NI} = T^{**} - \Delta T^{**}. \tag{3b}$$

The exponent α (the same in the N and I phases), both spinodal temperatures T^{**} and T^*, the B_C and D_C terms corresponding to the so-called heat capacity background, and the corresponding amplitudes $A_{C,N}$ and $A_{C,I}$ are found by fitting the experimental data of Fig. 4 to Eqs. (3a) and (3b). In the methodology followed, the common parameters in both phases (B_C, D_C, and α) have been simultaneously refined after a previous independent fitting. The most significant parameters ($A_{C,N}/A_{C,I}$, T^*, T^{**}, and α) that characterize the nature of the N-I phase transition are listed in Table II. All of the fitted parameters represent well the measured heat capacity data as is seen in Fig. 4 where both Eqs. (3a) and (3b) are drawn.

The latent heat associated with the N-I phase transition is calculated using Eq. (1) from the heat capacity data of Fig. 4. Our value is listed in Table I and is in quite good agreement with the value reported by Tripathi *et al.* [4].

The critical behavior of the scalar order parameter Q_N around the N-I phase transition as a function of temperature has been studied by calculating $Q'_N = (a_0/2T^*\rho_N)^{1/2}Q_N$, according to the methodology first used by others [34] and successfully applied by us elsewhere [32,33,35]. The scalar order parameter $Q_N(T)$ can be written as

$$Q_N^2(T) = \frac{2\,\rho_N T^*}{a_0}\left[\int_{T_I}^{T_{CI}} \frac{\Delta C_p}{T}dT + \frac{\Delta H_{NI}}{T_{NI}} + \int_{T_{CN}}^{T} \frac{\Delta C_p}{T}dT\right], \tag{4}$$

where ρ_N is the density of the liquid crystal in the nematic phases and the constant a_0 is the first coefficient in the Landau–de Gennes expansion [$A = a_0(T - T_0)/T_0$]. The integration of Eq. (4) has been made numerically on cooling from T_I in the isotropic phase, well above T_{NI}, at which Q_N could be considered zero down to T. Both temperatures, T_{CI} and T_{CN}, are the limiting temperatures of the coexistence region in the isotropic and nematic phases, respectively. The terms ΔH_{NI} and ΔC_p are the latent heat and the difference between the heat capacity and the heat capacity background, respectively. The Landau–de Gennes theory provides the generic expression [30]

$$Q'_N = Q'^{**}_N + K|T - T^{**}|^{\beta}, \quad \text{for } T < T^{**} - \Delta T.^* \tag{5}$$

The inset of Fig. 4 shows how well our calculated Q'_N data are fitted by Eq. (5) with a β critical exponent of 0.25 and the spinodal temperature T^{**} with the same value obtained through Eqs. (3a) and (3b) (see Table II).

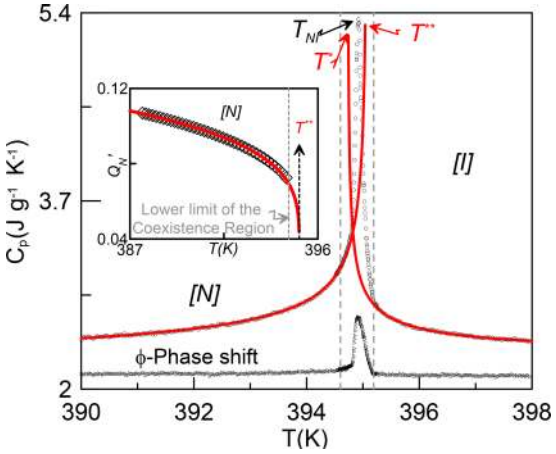

FIG. 4. (Color online) Heat capacity data as a function of temperature near the N-I phase transition. The limits of the heat capacity coexistence region (delimited by the vertical dashed lines) are defined by the phase shift angle data. Solid lines are fittings according to Eqs. (3a) and (3b). The inset shows Q'_N data as a function of temperature together with the corresponding fitting to Eq. (5).

2. *The N_{TB}-N phase transition*

Recently, some interesting models for the N_{TB}-N phase transition according to the Landau theory have been published [14,25,36]. In such models, the Oseen-Frank free energy is taken as the starting point for the modeling of a twist-bend nematic phase, but additional order parameters are required to account for the heliconical structure (tilt and twist) of the twist-bend nematic phase. Shamid *et al.* [14] propose a detailed approach based on the existence of polar order and bend coupling, i.e., a coupling which favors polar order along the bend. These theoretical approaches give rise to a second-order N_{TB}-N phase transition that, to date, has never been found. Experimental results for CB7CB, the most studied material exhibiting a twist-bend nematic-nematic phase transition, give a nonzero latent heat ($\Delta H_{N_{TB}N}$) [2] and an apparent discontinuity [37] of the conical angle, which, as in the Dozov Landau like model and molecular-field theory [26], is one of the possible order parameters characteristic of the N_{TB} phase. The latent heat ($\Delta H_{N_{TB}N}$) for the N_{TB}-N transition of CB9CB

TABLE II. Parameters of the fitting of the N_{TB}-N and the N-I phase transitions.

	N_{TB}-N		N-I			
Physical property	T_1 (K)	T_0 (K)	T^{**} (K)	T^{*} (K)	$A_{C,N}/A_{C,I}$	α
Heat capacity	379.3[a]	378.8[a]	395.1[a]	394.7[a]	1.6 ± 0.4	0.50 ± 0.05
Order parameter	–	–	395.1[a]	–	–	–

[a]The error in temperature is of ± 0.1.

was measured by Tripathi *et al.* [4] using high-resolution adiabatic calorimetry. In the present study, using the MDSC technique, $\Delta H_{N_{TB}N}$ is estimated using Eq. (1) from the heat capacity data of Fig. 5, and our value, listed in Table I, is in very good agreement with this. These results clearly indicate the first-order character of the N_{TB}-N phase transition. In addition, the data in Fig. 5 show an evident similarity to the heat capacity data around the N_{TB}-N phase transition for CB7CB, reported by us some years earlier [2]. At that time, the analysis of the critical behavior in the proximity of the N_{TB}-N phase transition was made by using the well-known and very simple phenomenological mean-field Landau model.

A very recent theoretical study made by Kats and Lebedev [38] argues that because of the short pitch of the helicoidal structure [7,22] the description of the N_{TB} phase based on the Oseen-Frank free energy requires modification and that the polar order should not be included. The chosen order parameter is a vector φ containing the conical angle and the pitch of the heliconical structure. Minimizing the proposed Landau functional with respect to the tilt angle and neglecting short-range fluctuations of the order parameter leads to the standard result of the mean-field Landau model. According to this study, the heat capacity of the twist-bend nematic phase close to the phase transition should be expressed as

$$C_p^{N_{TB}} = C_p^N + A^*[T_K - T]^{-1/2}, \tag{6}$$

where the heat capacity of the nematic phase (C_p^N) is described by the linear function

$$C_p^N = B^* + C^*[T - T_0]. \tag{7}$$

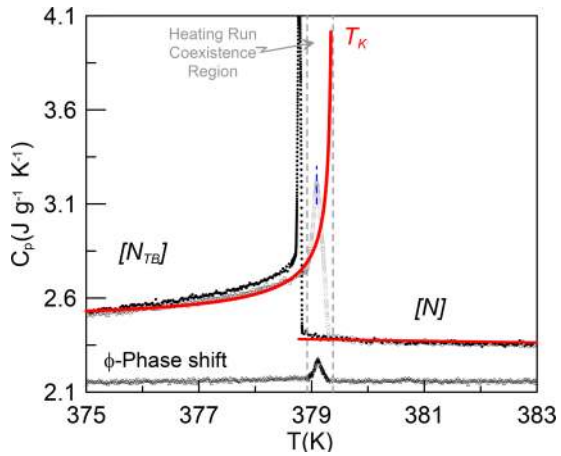

FIG. 5. (Color online) Heat capacity data as a function of temperature near the N-N_{TB} phase transition. The limits of the heat-capacity coexistence region (delimited by the vertical dashed lines) are defined by the phase shift angle data. Solid lines are fittings according to Eqs. (6) and (7).

The temperature T_K represents the temperature of the metastability limit for the twist-bend nematic phase on heating. The coefficients A^*, B^*, and C^* and the temperatures T_K and T_0 of both Eqs. (6) and (7) are obtained as fitting parameters from the experimental results of high-resolution heat capacity data in the vicinity of the N_{TB}-N phase transition, but close to the phase transition. In fact, there are two characteristic temperatures in the mean-field Landau model: The temperatures T_0 and T_1 are those at which second-order and first-order phase transitions take place, respectively. The temperature T_K is related to both T_0 and T_1 by means of the relationship

$$T_K = \tfrac{4}{3}T_1 - \tfrac{1}{3}T_0. \tag{8}$$

When the phase transition is considered tricritical, T_0 is set equal to T_1 and coincides with T_K.

Figure 5 shows the heat capacity for CB9CB in the vicinity of the N_{TB}-N phase transition (heating run: empty symbols; cooling run: full symbols) and the ϕ-phase shift data show a sharp peak which is a signature of the first-order character of the phase transition. This peak is used to determine the coexistence region (indicated by dashed lines in Fig. 5). Our heat capacity data have been fitted to Eqs. (6) and (7) and both equations are drawn (red lines) in Fig. 5. The two characteristic temperatures, T_0 and T_1, are listed in Table II. The key result from our fit is the value of $T_K/T_0 = 1.0018$ and using Eq. (8), $T_1/T_0 = 1.0014$. Both temperature ratios are compatible with a first-order N_{TB}-N phase transition, but one which is nearly tricritical. For the shorter-chain homologue, CB7CB, this transition was analyzed according to the same theoretical model and the results are similar [2], though the longer spacer in CB9CB will be expected to influence the details of the transitional behavior. These results point to a first-order phase transition although with a strength that changes with the molecular structure, such as the spacer length [2,8]. Thus, for CB9CB the associated latent heat of the N_{TB}-N phase transition is about 125 J mol^{-1} whereas for CB7CB it is about 205 J mol^{-1}.

B. Dielectric studies

In liquid crystal dimers, molecular flexibility provided by the spacer, and the corresponding changing distribution of conformers, has a major effect on the energetically favored molecular shapes and thus, on the mesophase properties [39,40]. The conformational distribution is also influenced by the anisotropic nematic interactions, favoring molecular geometries that can better adapt to the nematic ordering and environment. The temperature dependence of the dielectric response of a liquid crystal phase depends on the rotational distribution of the molecular dipoles in the presence of an

electric field and the orientational order of the phase. However, the order parameter itself is temperature dependent, and, as indicated previously, both the molecular dipoles, through the shape, and the order parameter are affected by the conformational distribution.

Calculations of the conformational energy as a function of the angle between the two terminal mesogenic groups have been carried out using a continuous torsional potential for the flexible chain segments. The results have shown that the CB7CB homologue has a temperature dependent conformational distribution characterized by a strong, broad peak centered around 120° (extended conformers) and a weak peak at 30° (hairpin conformers) [2]. These calculations also show that the increase of the orientational order parameter is accompanied by the growth of the proportion of extended conformers and in addition, by a slight increase of the angle between mesogenic units; i.e., the average molecular shape is adapting to the increased orientational order in the nematic environment [41].

Electric dipoles can be used as effective molecular probes to detect changes in molecular structure via dielectric measurements. Dielectric permittivity provides a measure of the averaged molecular mean-square dipole moment, which is determined by the conformationally averaged vector sum of the constituent dipoles and, hence, is directly related to the distribution of molecular conformations [15,42–44]. For the dimers CB7CB and CB9CB, the mean-square dipole moment is given by the averaged vector sum of the dipole moments associated with the nitrile groups attached to the terminal mesogenic units. The different molecular conformers will contribute differently to the measured components of the dielectric permittivity. Thus the extended conformers having an angle between the terminal dipoles of around 120° will have a zero mean-square dipole component contributing to the parallel permittivity along the director. For such conformers there will be a nonzero contribution (transverse) of the dipoles to the perpendicular component of the permittivity, which will depend on the angle between the terminal dipolar groups. Hairpin conformers will have a large mean-square dipole moment contribution to the parallel permittivity measured along the director. Furthermore, the relaxation rates for the transverse and longitudinal dipole polarizations are different, and so changes of the conformational distribution of the interarm angle should be clearly reflected by measurements of the dielectric permittivity.

We have performed measurements of the parallel and perpendicular static dielectric permittivity components of CB9CB on cooling from the isotropic phase. The perpendicular component of the permittivity ($\varepsilon_\perp$) was directly obtained using harmonic probe fields of low amplitude (0.5 V_{rms}) well below the threshold voltage of the Fréedericksz transition. On the other hand, the parallel component ($\varepsilon_{||}$) was measured by applying voltages well above the transition, which aligns the director parallel to the field. Both components were measured as a function of temperature at various frequencies. Results show that capacitance measurements are significantly influenced by undesired ionic effects for frequencies below 5 kHz, particularly for the parallel component, and so the static dielectric permittivity was determined at 5 kHz as shown in Fig. 6(a). This frequency is well below the characteristic

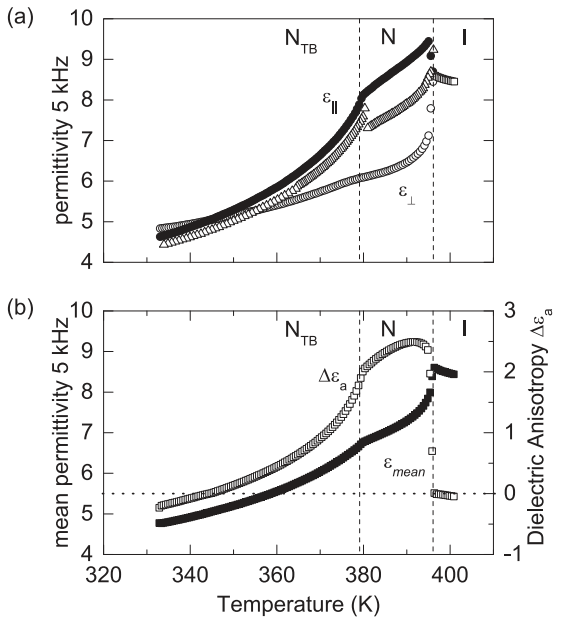

FIG. 6. (a) Temperature dependence of the static permittivity: (□) isotropic phase, (○) perpendicular component, and (•) parallel component. Open triangles (△) correspond to the parallel component of the permittivity measured with dc bias in metallic cells. (b) Temperature dependence of the (■) mean permittivity and (□) dielectric anisotropy.

frequency of the lowest relaxation over the whole temperature range as will be shown later. Additionally, the mean dielectric permittivity [$\bar{\varepsilon} = (\varepsilon_{||} + 2\varepsilon_\perp)/3$] and the dielectric anisotropy ($\Delta\varepsilon_a = \varepsilon_{||} - \varepsilon_\perp$) are shown in Fig. 6(b) as a function of temperature. Open triangles in Fig. 6(a) represent the static dielectric permittivity obtained with metallic cells under dc bias conditions. Static dielectric permittivity measurements for CB9CB show a temperature dependence similar to that reported for other symmetric dimers [2,6,42] and clearly reflect the phase transitions detected optically and by calorimetric studies. As expected for materials with positive dielectric anisotropy, the value of the perpendicular component of the permittivity decreases on cooling from the isotropic phase while the parallel component increases at the isotropic-to-nematic transition. For odd dimers, this increase can be explained in terms of the slight stabilization of hairpin conformers at the onset of nematic ordering. However, after this initial growth the parallel permittivity starts to decrease in the nematic phase on further reducing the temperature. As can be observed in Fig. 6(b), this trend entails a progressive increase of the difference between the mean permittivity and the extrapolated isotropic value with decreasing temperature, i.e., a significant reduction of the average molecular mean-square dipole moment as the orientational order of the phase increases. As mentioned before, this fact can be explained satisfactorily by the progressive increase in the population of extended conformers with zero longitudinal dipole moment, which is driven by the increase of orientational order [41].

On entering the N_{TB} phase, the decrease with lowering temperature of both components of the permittivity is accelerated,

and at low temperatures there is a sign reversal in the dielectric anisotropy from positive to negative.

1. Permittivity measurements as a function of temperature and frequency

To gain insight into the rotational dynamics of the dipolar groups, measurements of the frequency dependent dielectric permittivity were made. The interpretation of the dielectric absorption of dimers as a function of frequency has required the development of a suitable theoretical model based on a time-scale separation between the motion of the mesogenic units and the fast relaxation of the flexible chain [41]. This model assumes that the molecular reorientation occurs via the individual orientational relaxation of the mesogenic units (end-over-end processes) and excludes whole molecule reorientation, which would require the simultaneous reversal of both terminal groups, for which the corresponding energy barrier is too high. For symmetric dimers, such as CB9CB, a single low-frequency absorption whose strength depends on the population distribution of conformers is predicted.

The dynamic dielectric response of CB9CB was investigated in 50-μm-thick metallic cells under two dc bias conditions (0 and 35 V). As will be shown later, in measurements without dc bias, metal surface interactions induce planar alignment allowing us to obtain the perpendicular component of the permittivity. The application of a dc bias reorients the sample and the permittivity saturates at high voltages. Results obtained for the static permittivities of CB9CB using both the 8-μm glass Instec cell and the 50-μm metal cell are shown in Fig. 6. From the comparison of the parallel static permittivity components given in Fig. 6(a), it is clear that the alignment obtained in 50-μm cells with dc bias is not equivalent to that achieved in 8-μm cells with ac bias. Textures observed when applying a dc bias in glass cells indicate that the divergence between both alignments can be assigned to director fluctuations caused by convective instabilities. For the variable frequency measurements, it is only possible to obtain values for the parallel component of the permittivity ($\varepsilon_{||}$) from 50-μm metal cells with dc bias. The frequency dependence of the real and imaginary parts of the perpendicular and parallel dielectric permittivity components are given, respectively, in Figs. 7 and 8 for temperatures in the nematic and twist-bend nematic phases. The dielectric response of CB9CB in the nematic phase, like that of its homologue CB7CB, is characterized by two relaxation processes whose contribution to the dielectric spectrum depends on the alignment of the director in the measurement cell. These dielectric relaxations can be associated with the rotational diffusion of the dimer molecules: an end-over-end reorientation of the dipolar groups parallel to the director at low frequencies (m_1), in agreement with the theoretical model for dielectric relaxation in nematic dimers [40], and the precessional motion of the dipolar groups around the director for the high-frequency branch of the spectrum (m_2). The frequency and temperature dependences of the dielectric absorption, represented as three-dimensional plots, are given for both alignments in Fig. 7(a) (perpendicular to **n**) and Fig. 8(a) (parallel to **n**).

For each temperature and director alignment the frequency dependence of the permittivity has been analyzed by fitting

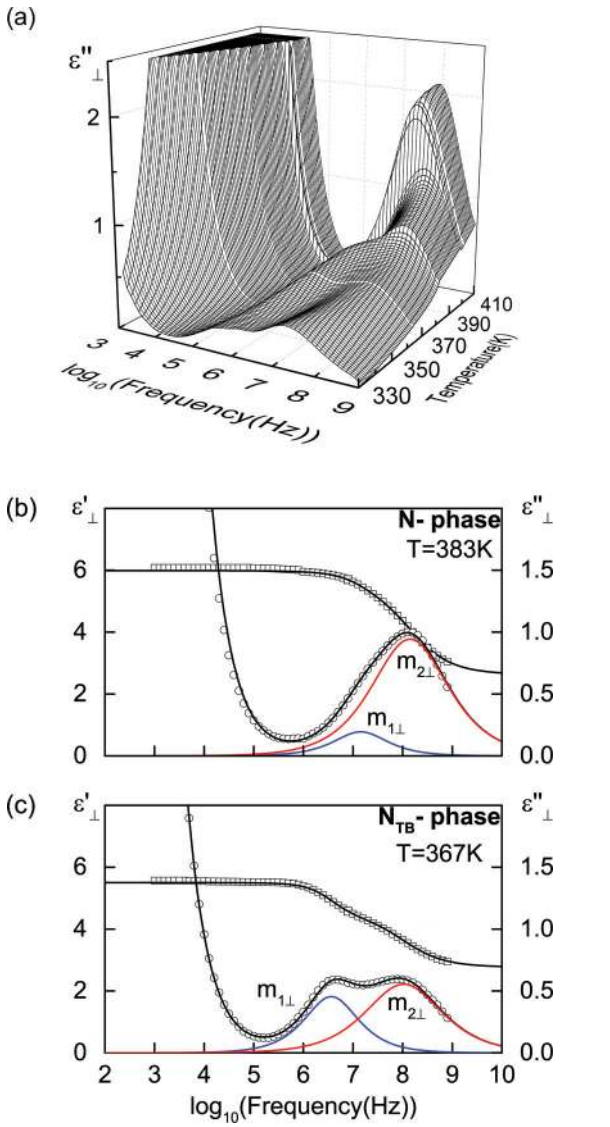

FIG. 7. (Color online) Perpendicular alignment. (a) Three-dimensional plot of the dielectric losses vs temperature and logarithm of the frequency. Frequency dependence of $\varepsilon'_\perp$ (□) and $\varepsilon''_\perp$ (○) (b) in the N phase, and (c) in the $N_{\rm TB}$ phase. In (b) and (c) solid lines are fits to Eq. (9).

each relaxation mode according to the Havriliak-Negami function through the empirical relationship

$$\varepsilon(\omega) - \varepsilon_\infty = \sum_{k=1,2} \frac{\Delta\varepsilon_k}{[1 + (i\omega\tau_k)^{\alpha_k}]^{\beta_k}} - i\frac{\sigma_{\rm dc}}{\omega\varepsilon_0}, \qquad (9)$$

where ε_∞ is the extrapolated high-frequency permittivity, $\Delta\varepsilon_k$ is the strength of the corresponding relaxation mode, and $\sigma_{\rm dc}$ is the dc conductivity. The relaxation time τ_k is related to the frequency of maximum loss through the parameters α_k and β_k, which describe the width and the asymmetry of the relaxation spectra, respectively ($\alpha = \beta = 1$ corresponds to a simple Debye-like process). As an example, fittings for both director alignments are given in Figs. 7(b) ($\perp$**n**, N), 7(c) ($\perp$**n**, $N_{\rm TB}$), 8(b) (||**n**, N), and 8(c) (||**n**, $N_{\rm TB}$). Measurement results were fitted by assuming two relaxation processes,

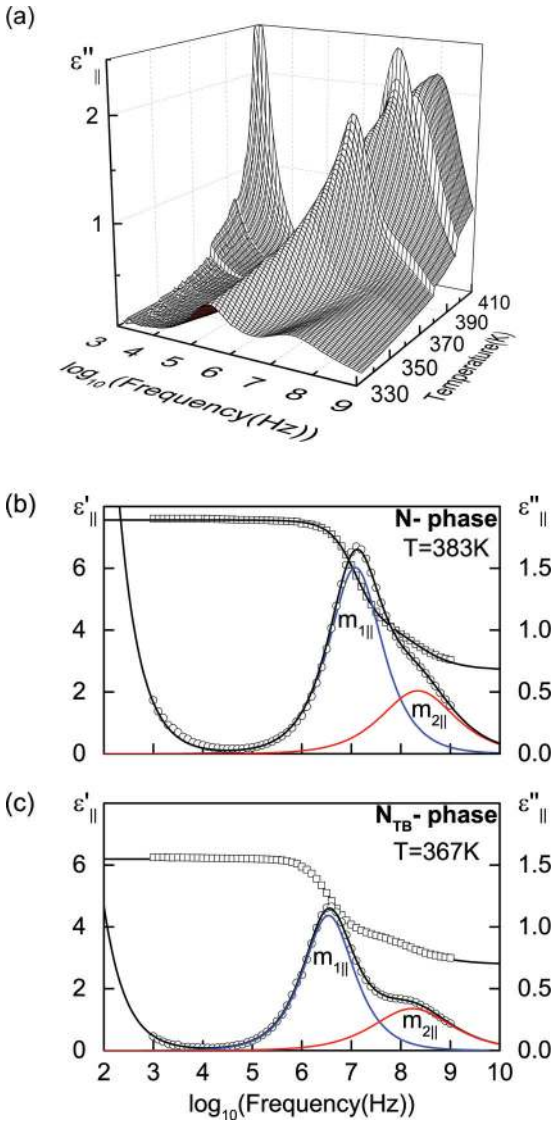

FIG. 8. (Color online) Parallel alignment. (a) Three-dimensional plot of the dielectric losses vs temperature and logarithm of the frequency. Frequency dependence of $\varepsilon'_{||}$ (□) and $\varepsilon''_{||}$ (○) (b) in the N phase and (c) in the N_{TB} phase. In (b) and (c) solid lines are fits to Eq. (9).

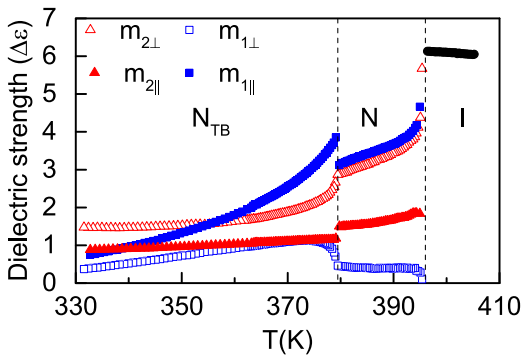

FIG. 9. (Color online) Dielectric strength of the relaxation modes vs temperature: full symbols, parallel alignment, empty symbols, perpendicular alignment; (•) isotropic phase, (■,□) low-frequency mode in the N and N_{TB} phases, (▲,△) high-frequency mode in the N and N_{TB} phases.

approximately a Cole-Cole shape, having α about 0.95 for m_1 and 0.75 for m_2 in both nematic phases.

Dielectric strengths for each relaxation are given as a function of temperature in Fig. 9. As observed also in the three-dimensional plot (see Fig. 7), for the perpendicular component of the permittivity, the high-frequency mode ($m_{2\perp}$) dominates over the temperature range of the nematic phase. There is a minor contribution from the low-frequency mode ($m_{1\perp}$), but its very low strength allows us to attribute it to a very small amount of director misalignment in the planar configuration. Conversely, for the parallel alignment the dielectric spectrum is dominated by the low-frequency relaxation ($m_{1||}$, end-over-end reorientation), with a smaller contribution from the high-frequency mode ($m_{2||}$) (see Fig. 9). Although this behavior would be expected for the parallel director configuration, the rapid decrease of the low-frequency mode strength ($\Delta\varepsilon_{m1||}$) implies a much steeper reduction of the static permittivity than that found in the glass cells [see Fig. 6(a)]. As we have already indicated, this behavior is attributed to the inhomogeneous director distribution caused by electroconvective instabilities.

As already noted for CB7CB [2], at the N-N_{TB} transition, on lowering the temperature, the contribution of the low-frequency mode ($m_{1\perp}$) to the perpendicular component of the permittivity shows an abrupt increase. This is clear from Figs. 7(a) and 9, where the strength of the low-frequency mode ($m_{1\perp}$) shows a rapid increase below the N-N_{TB} transition. Such a sharp growth can be explained by the sudden tilt of the average axis of the longitudinal dipole moment, compatible with the heliconical director distribution. The dielectric strengths are obtained from a deconvolution of the frequency dependent dielectric response, as indicated in Fig. 7, and because of this it is not possible to determine if the apparent change in the strength is discontinuous or continuous, but the change in the appearance of the spectra is dramatic. Meanwhile, the strength of the predominant mode $m_{2\perp}$ undergoes a small decrease at the transition and then reduces more slowly at lower temperatures. Regarding the parallel configuration, the low-frequency contribution experiences an increase at the N-N_{TB} transition and the resulting value of the static permittivity is almost the same as that obtained with glass cells and ac voltages [see Fig. 6(a), full symbols]. A simple and tentative explanation for this behavior can be given in terms of the sharp decrease of the sample conductivity at the transition to the twist-bend nematic phase, which will hinder director fluctuations and allow for the realignment of the director parallel to the field.

An Arrhenius plot of the temperature dependence of the characteristic relaxation frequencies associated with each mode is given in Fig. 10. The analysis of these relaxation frequencies yields another interesting observation. While the dielectric amplitudes of the relaxation processes experience clear jumps at the N-N_{TB} transition, the corresponding frequencies remain almost unaltered showing a slight decrease for the end-over-end rotation and a comparable increase for the high-frequency mode. In addition, the activation energy for the end-over-end process is found to be almost unaltered

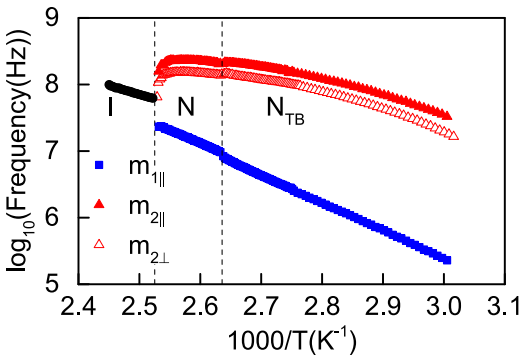

FIG. 10. (Color online) Arrhenius plot of the frequency of the relaxation modes: full symbols, parallel alignment, empty symbols, perpendicular alignment; (•) isotropic phase, (■) low-frequency mode in the N and N_{TB} phases, (▲,△) high-frequency mode in the N and N_{TB} phases.

at the transition, being about 76 kJ mol^{-1} in both nematic phases.

Recent studies on CB7CB [17,37] reported values of the tilt angle of the director, estimated from birefringence measurements. In the heliconical N_{TB} phase, the tilt angle shows a very steep increase near the phase transition which is followed by a less rapid increase when it reaches more than 35° at just over 50 °C below the N-N_{TB} transition [37]. Similar values are estimated from ^{2}H NMR results for CB7CB [21]. However, more recent NMR studies of CB7CB using ^{129}Xe as a spin probe based on a recently proposed model for the analysis of the chemical shift shows that the conical angle exhibits a less rapid increase on entering the N_{TB} phase [45]. This is a puzzling observation to which we shall return shortly. In our dielectric characterization of the twist-bend nematic phase, we claim that the observation of a sudden increase in the contribution of the low-frequency (end-over-end) relaxation $m_{1\perp}$ to the measured perpendicular dielectric absorption at the N-N_{TB} transition is consistent with the rapid development of a director tilt, which would be expected and has been seen on the formation of a heliconical phase. This, in principle, provides a method to estimate values of the tilt angle for CB9CB from our dielectric measurements.

For the purposes of estimating the tilt angle in the twist-bend nematic phase, we assume that the dielectric strength ($\Delta\varepsilon_{m1\perp}$) of $m_{1\perp}$ in the twist-bend nematic phase is due only to the director tilt (θ_0) with respect to the heliconical axis, and that the order parameter does not change at the transition. Then the value of $\Delta\varepsilon_{m1\perp}$ in the twist-bend phase is the appropriate component of the dielectric strength measured for this relaxation in the absence of tilt $\Delta\varepsilon_{m1||}$ rotated by the tilt angle; $\Delta\varepsilon_{m1||}$ is the dielectric strength as measured in the nematic phase ($\theta_0 = 0$), for the parallel component of the absorption. Since the components of the dielectric strength behave as second rank tensors, the relation between the value $\Delta\varepsilon_{m1\perp}$ in the twist-bend phase measured perpendicular to the heliconical axis and the value for zero tilt $\Delta\varepsilon_{m1||}$ measured along the alignment axis is $\Delta\varepsilon_{m1\perp} = \Delta\varepsilon_{m1||}\sin^2\theta_0$. At 6 K below the N-N_{TB} transition the value of $\Delta\varepsilon_{m1\perp}$ is 1.1, while the value of $\Delta\varepsilon_{m1||}$ is 4. This value has been rescaled to take account of the small misalignment in the 50-μm metal cell due to convective instabilities in the nematic phase already discussed. Neglecting any changes in the orientational order parameter at the N-N_{TB} transition, this gives a tilt angle of 30° for CB9CB in the twist-bend phase 6 K below the N-N_{TB} transition, similar to that already reported for CB7CB [17,37].

2. *Elastic constants from electric-field induced realignment*

As Dozov proposed theoretically [12], spontaneous stabilization of the predicted lower local symmetry nematic phases with splay-bend or twist-bend modulation can result from a negative bend coefficient K_3. In addition, it was shown that the difference in the elastic free energy between the two possible modulated nematic mesophases imposes the inequality $K_1 > 2K_2$ for the splay and twist elastic constants in order for the twist-bend distortion to be energetically favorable with respect to the splay-bend phase. Therefore, investigations of the elastic properties are directly related to the experimental identification of such spontaneously modulated nematic phases. In order to explore the possible stabilization of a twist-bend nematic phase, a number of studies have examined the elastic properties of the higher temperature nematic phase [6,7,9,46] for materials that exhibit the twist-bend nematic phase. These include (i) molecular-field calculations for the shorter dimer, CB7CB, suggesting that the condition $K_1 > 2K_2$ is fulfilled [2] and (ii) experimental determination of splay and bend elastic constants, but not the twist elastic constant, for the nearest longer dimer CB11CB [6]. In Ref. [46] measurements of K_1, K_2, and K_3 for CB7CB in both the nematic and the twist-bend nematic phases are reported. The value they found for the ratio K_1/K_2 was around 1.4 in the N phase but the most intriguing result is the huge increase of K_3 and the decrease of K_1 on entering the N_{TB} phase. This is explained as being due to a different nature of the elastic distortions near the N_{TB}-N phase transition [46].

We have determined the splay and bend elastic constants in the nematic phase of CB9CB by measuring the change in the capacitance when a variable voltage is applied to planar aligned samples of the nematic director. The frequency of the applied electric field was set equal to 5 kHz, as for measurements of the static permittivity, to avoid undesired ionic effects. Careful analysis of the data was performed at a series of temperatures by fitting the capacitance vs voltage curve to the following equations [47]:

$$V = \frac{2V_{th}}{\pi}\sqrt{1+\gamma\eta}\int_{\psi_0}^{\pi/2}\left[\frac{1+\kappa\eta\sin^2\psi}{(1+\gamma\eta\sin^2\psi)(1-\eta\sin^2\psi)}\right]^{1/2}d\psi, \tag{10a}$$

$$C = C_\perp\frac{\int_{\psi_0}^{\pi/2}\left[\frac{(1+\gamma\eta\sin^2\psi)(1+\kappa\eta\sin^2\psi)}{(1-\eta\sin^2\psi)}\right]^{1/2}d\psi}{\int_{\psi_0}^{\pi/2}\left[\frac{1+\kappa\eta\sin^2\psi}{(1+\gamma\eta\sin^2\psi)(1-\eta\sin^2\psi)}\right]^{1/2}d\psi}. \tag{10b}$$

Here the parameter η is related to the maximum tilt angle at the center of the cell ϕ_m through the relation $\eta = \sin^2(\phi_m)$; the parameters γ and κ correspond to the reduced quantities $\gamma = C_\perp/C_{||} - 1$ and $\kappa = K_3/K_1 - 1$.The capacitance for perpendicular director alignment, $C_\perp$, was deduced from the capacitance of the cell before the onset of the Fréedericksz transition, V_{th}. The capacitance for parallel director alignment,

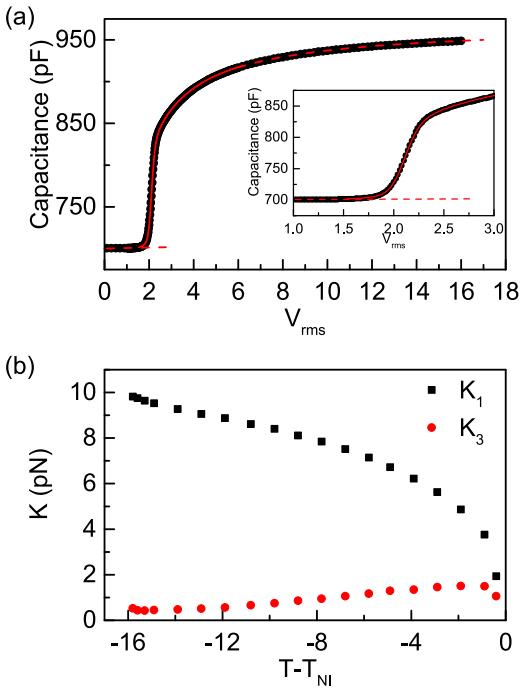

FIG. 11. (Color online) (a) Voltage dependence of the capacitance recorded at 5 kHz for the shifted temperature $T - T_{NI} = -13$ K. Solid line shows the theoretical fit to Eqs. (10a) and (10b). (b) Temperature dependence of the elastic constants K_1 and K_3 in the nematic phase.

$C_{||}$, was determined from the extrapolated capacitance in the limit of a very large aligning field $1/V \to 0$ [48]. In order to obtain the threshold voltage V_{th} and κ, capacitance data above the threshold voltage were fitted to Eqs. (10a) and (10b) based on a least squares minimization procedure. These values of V_{th} and κ were employed to calculate K_1 and K_3 using the relationship

$$K_1 = (V_{th}/\pi)^2 \varepsilon_0 \Delta\varepsilon. \tag{11}$$

Before fitting over the entire temperature range, tests for different values of the pretilt angle, α, in the range of $0°-3°$, were performed by introducing in Eqs. (10a) and (10b) the integral limit value $\psi_0 = \arcsin[\sin\alpha/\sqrt{\eta}]$. Even though not too great a difference was observed, the best and final fittings were performed for $\alpha = 2.2°$. An example of the voltage variation of the capacitance together with the corresponding fitting is plotted in Fig. 11(a) for a temperature close to the N-N_{TB} transition.

The splay and bend elastic constants are shown in Fig. 11(b) as a function of temperature. The results show that the splay elastic constant, K_1, increases with decreasing temperature while the bend elastic constant, K_3, which is significantly smaller than K_1, decreases with decreasing temperature, after an initial increase at the N-I transition, reaching values as small as 0.43 pN, before increasing slightly as found for other systems [9]. Such a decrease is in good agreement with earlier theoretical predictions [11] and the results are comparable to experimental determinations for other odd liquid crystal dimers exhibiting a twist-bend nematic phase [9,10,15,49]. The results for CB9CB reported here, for both K_1 and K_3, have slightly higher values than for the previously reported homologue CB7CB [25,49], but for the longer analogue CB11CB [6] both K_1, but above all K_3, are much higher. This difference may be attributed to the effect the length of the linking chain has on the molecular shape or also to a different experimental methodology. The shorter chains for CB9CB and CB7CB would enhance the bent molecular structure of the dimer with respect to that of the undecane homologue, significantly reducing K_3. Our measurements for CB7CB [49] in the N phase are comparable to those reported in Ref. [46] for K_1, but our value for K_3 near the N_{TB} phase is slightly larger (0.43 pN vs 0.3 pN) and of the same order as for CB9CB. It is important to note that in the analysis, the splay elastic constant depends on the assumed value for the dielectric anisotropy at the measurement frequency. This was carefully selected to avoid spurious low-frequency ionic contributions that tend to increase the permittivity and thus to overestimate K_1 values.

The temperature dependence of K_3, and in particular its maximum near T_{NI}, require further analysis. Similar behavior has been found for liquid crystal mixtures of bent-core and rodlike molecules with a sufficiently high concentration of bent-core molecules [50,51]. As proposed in these cases, the initial increase of K_3 could be related to the increase of the order parameter, whereas its further decrease would arise from the better coupling of the bent shape of the molecules to a bend distortion of the director, depending on the bend angle. However, for liquid crystal dimers it is important to recall that the internal flexibility of the molecules leads to a temperature dependent conformational distribution. The similarity between the dielectric anisotropy [Fig. 6(b)] and the bend elastic constant [Fig. 11(b)] supports the assumption that the temperature dependence of the conformational distribution should not be disregarded when analyzing the behavior of K_3.

C. ^{2}H NMR spectroscopy: Chirality, order parameters, and conical angle

The aim of the NMR experiments is to explore the orientational order of both nematic phases, and for the twist-bend nematic phase its chirality and conical angle, and how they vary with temperature. A selection of deuterium NMR spectra is shown in Fig. 12. In the nematic phase at 380 and 377 K the spectra show a single quadrupolar doublet consistent with the achirality of the phase and the alignment of the director by the magnetic field. Careful examination of the spectra reveals a weak quadrupolar doublet which has been associated with a partially deuterated dimer impurity; this single doublet is more apparent in the N_{TB} phase [45]. For the spectrum in the nematic phase at 377 K the spectral lines broaden slightly, consistent with the approach of the N_{TB} phase with its higher viscosity. In the twist-bend nematic phase the two spectra at 376 and 363 K contain two quadrupolar doublets which provide a clear demonstration of the phase chirality, to be discussed later. The spectra were measured carefully on going through the N_{TB}-N phase transition, and the change in the spectral linewidths is consistent with a weak first-order phase transition and an almost continuous change in the mean of the prochiral quadrupolar splittings.

The temperature variation of the quadrupolar splittings for the probe CB7CB-d_4 dissolved in the dimer CB9CB are

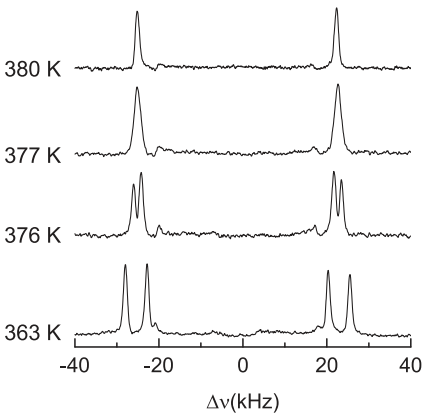

FIG. 12. The ^{2}H NMR spectra of CB7CB-d_4 dissolved in CB9CB at four temperatures, two in the nematic phase and the lower two in the twist-bend nematic phase.

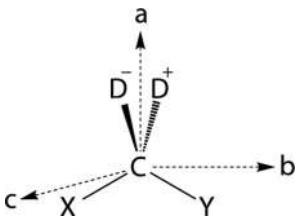

FIG. 14. The conformationally averaged structure of CB7CB-d_4 with the reference frame set in one of the methylene, CD_2, fragments. The coordinate system a, b, c is also shown together with the averaged groups X (in the spirit of the model the X cyanobiphenyl group is not averaged because C-X is parallel to the para-axis of the cyanobiphenyl group also known as cyanobiphenyl) and Y (also known as the spacer and second cyanobiphenyl group). The mirror plane at the methylene group is in the plane of the paper, i.e., the plane defined by XCY. In a chiral environment, such as a twist-bend nematic, this symmetry plane is removed, and the atoms D+ and D−, above and below the plane of the paper, become inequivalent.

shown in Fig. 13. Although the splittings are for the probe, its low concentration and structural similarity to the host should ensure that they reflect the orientational order of CB9CB. In the N phase we see the initial, normal growth of this order with decreasing temperature. As the N_{TB} phase is approached, so the rate of increase diminishes and the splitting essentially reaches a plateau which is unusual [9]. On entering the twist-bend nematic two doublets are clearly apparent, and this loss of equivalence of the prochiral deuterons results from the loss of the plane of symmetry in the averaged molecule caused by the chirality of the low temperature nematic phase (see Fig. 14) [2]. This provides a clear indication of the identity of the N_{TB} phase. The difference in the two quadrupolar splittings grows with decreasing temperature and might be associated with a change in the N_{TB} phase structure. However, molecular-field theory predicts that although the pitch decreases rapidly in the N_{TB} phase after the transition, it then changes relatively slowly at lower temperatures [26]. In marked contrast to the behavior of this chiral splitting the mean quadrupolar splitting is more or less independent of temperature. To understand this, at least qualitatively, we recall that with decreasing temperature the orientational order should grow, as should the conical angle. Whereas the increasing order causes the quadrupolar splitting to increase, increasing the conical angle results in a decrease of the splitting. It seems that these two effects essentially balance throughout the N_{TB} phase as can be seen in Fig. 15.

A more quantitative interpretation of the NMR splittings can be obtained by relating them to the Saupe ordering matrix for the CB7CB dimer, details of which have been given by Beguin *et al.* [18]. The rigid fragments containing the prochiral deuterons are in the first and last methylene groups in the heptane spacer, which for CB7CB-d_4 are equivalent. These are now used as reference frames and allow us to include the molecular flexibility associated with the spacer. By taking an average over all molecular conformers, the system can be treated as the averaged structure sketched in Fig. 14. Attached to the carbon atom of a CD_2 unit are two nonequivalent groups: X represents a cyanobiphenyl group, while Y is the methylene spacer attached to the second terminal cyanobiphenyl group averaged over all conformers. The plane formed by X, C, and Y is a mirror plane and the c axis is orthogonal to this; the a axis bisects the DĈD bond angle and is orthogonal to c; the b axis is orthogonal to a and c. In this frame the Saupe ordering matrix, which we shall refer to as the averaged Saupe matrix, takes the form

$$\mathbf{S} = \begin{pmatrix} S_{aa} & S_{ab} & 0 \\ S_{ab} & S_{bb} & 0 \\ 0 & 0 & S_{cc} \end{pmatrix}. \tag{12}$$

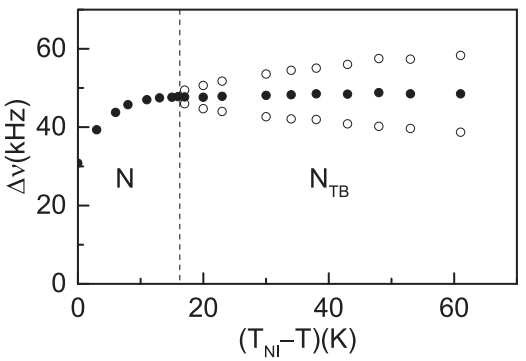

FIG. 13. The dependence on the shifted temperature, T_{NI}-T, of the quadrupolar splittings for the probe, CB7CB-d_4, doped in the nematic and twist-bend nematic phases of the host, CB9CB.

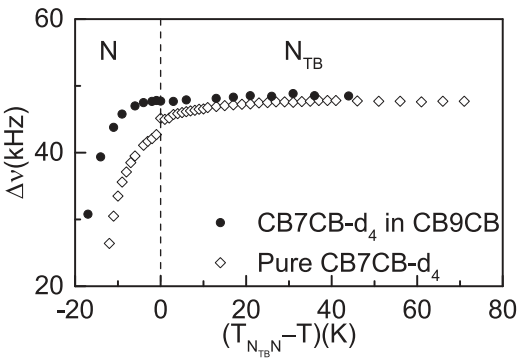

FIG. 15. The variation of the mean quadrupolar splitting with the shifted temperature, $T_{N_{TB}N}$-T, for CB7CB-d_4 doped in CB9CB (•) and for CB7CB-d_4 (◇).

The key quantities of relevance here are the quadrupolar splittings for the two deuterons and these are

$$\Delta\nu_+ = (3/2)q_{\rm CD}S_{\rm CD+}, \tag{13a}$$

$$\Delta\nu_- = (3/2)q_{\rm CD}S_{\rm CD-}, \tag{13b}$$

where $q_{\rm CD}$ is the component of the quadrupolar tensor parallel to the C-D bond, assuming the local symmetry to be cylindrically symmetric about the bond. Because of the mirror plane symmetry, the order parameters for the two C-D bonds denoted $S_{\rm CD+}$ and $S_{\rm CD-}$ are equal, and Beguin *et al.* [18] have shown that these two order parameters can be written in terms of the elements of the averaged Saupe matrix as

$$S_{\rm CD+} = S_{aa}\cos^2\beta + S_{cc}\sin^2\beta = S_{\rm CD-}, \tag{14}$$

where β is the angle between a C-D bond and the a axis. The quadrupolar splitting measured in the nematic phase is proportional to two diagonal elements of the Saupe matrix and one of these, S_{cc}, is a principal component.

The chirality of the twist-bend nematic phase means that the mirror plane for the methylene group is lost and all elements of the averaged matrix are nonzero. Of particular significance is the off-diagonal element S_{ac}, as a result of which the two C-D bonds are no longer equivalent and the relevant order parameters are now

$$S_{\rm CD+} = S_{aa}\cos^2\beta + S_{cc}\sin^2\beta + S_{ac}\sin 2\beta, \tag{15a}$$

$$S_{\rm CD-} = S_{aa}\cos^2\beta + S_{cc}\sin^2\beta - S_{ac}\sin 2\beta. \tag{15b}$$

The label + or − is seen to relate to the sign of the term in S_{ac} in the expression for the order parameters of the C-D bonds. We can see that by taking the mean of the quadrupolar splittings in the $N_{\rm TB}$ phase then via Eqs. (13) and (15) this sum is given by

$$(\Delta\nu_+ + \Delta\nu_-)/2 = (3/4)q_{\rm CD}(S_{aa}\cos^2\beta + S_{cc}\sin^2\beta), \tag{16}$$

which is equivalent to the quadrupolar splitting in the nematic phase [see Eq. (14)]. It is then the mean splitting in the $N_{\rm TB}$ phase which should be compared with the splitting in the nematic phase as we have done in Fig. 15. The results, shown in Eqs. (15a) and (15b), also indicate that the off-diagonal element, S_{ac}, is related to the difference in the quadrupolar splittings by

$$(\Delta\nu_+ - \Delta\nu_-)/2 = (3/4)q_{\rm CD}S_{ac}\sin 2\beta. \tag{17}$$

We refer to this difference as the chiral splitting, and it is zero in an achiral system, for which the off-diagonal element S_{ac} of the averaged Saupe matrix vanishes.

In Figs. 15 and 16, the results for the mean quadrupolar splitting and the chiral quadrupolar splitting, respectively, for CB7CB-d_4 dissolved in CB9CB are compared with those for pure CB7CB-d_4 [2]. Since the two systems have different transition temperatures, we have used a shifted temperature scale with respect to the transition temperature, $T_{N_{\rm TB}N}$. The results for CB7CB-d_4 dissolved in CB9CB clearly show that the splitting in the nematic phase is almost continuous with the mean splitting in the twist-bend nematic as well with as the pretransitional plateau in the nematic phase prior to the formation of the $N_{\rm TB}$ phase. This behavior is in contrast to that of the lower homologue CB7CB, where there is a clear discontinuity in the splittings for the two phases. This suggests

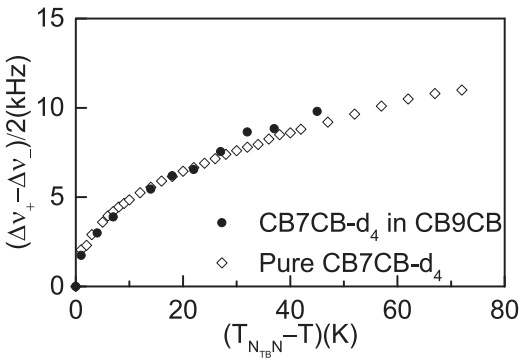

FIG. 16. The variation of the chiral quadrupolar splitting with the shifted temperature, $T_{N_{\rm TB}N}$-T, for CB7CB-d_4 doped in CB9CB (•) and for CB7CB-d_4 (◇).

that the first-order $N_{\rm TB}$-N transition for CB7CB is stronger than that for CB9CB, which is much closer to second order, for which there would be no discontinuity. The strength of this transition may be related to the length of the N phase prior to the formation of the $N_{\rm TB}$ phase analogous to the behavior of the Sm-A−N transition [52]. In Fig. 16, the temperature dependence of the chiral splitting for CB9CB is compared with that for its shorter homologue CB7CB. On the shifted temperature scale, the results are very similar, except that the chiral splitting is apparently zero, to within experimental error, for CB9CB at the transition temperature $T_{N_{\rm TB}N}$, while there is a small but significant jump for CB7CB indicating a difference in the strength of the transition for the two dimers. This difference may well result from the change in the curvature of their average structures [26].

The two prochiral quadrupolar splittings of the probe molecule 8CB-d_2 dissolved in CB7CB have been used to estimate the helical pitch of the host and the conical angle of the director [21]. This determination is based on a model for the director distribution in the $N_{\rm TB}$ phase, its relation to the molecular conformation to give the orientational order and the quadrupolar splittings of the prochiral deuterons. More recently ^{129}Xe has been used as an NMR probe to explore the structure of the N and $N_{\rm TB}$ nematic phases for CB7CB [45]. This experiment yields a single peak which gives the shielding or chemical shift and a model has been developed to determine both the conical angle and the orientational order parameter of the cyanobiphenyl group with respect to the director. To achieve this, analytic expressions have been proposed to describe the temperature dependence in the $N_{\rm TB}$ phase of the orientational order parameter and the conical angle. Here we shall use the same approach to obtain this information from the mean quadrupolar splitting for the probe CB7CB-d_4 in CB9CB.

To understand how the probe molecule CB7CB-d_4 used in our NMR experiments is ordered, it is helpful to envisage the conformational average it will adopt on the NMR time scale. It has been thought that the average shape of an odd dimer would have a bent core, especially as this is required for the formation of the twist-bend nematic phase [37]; indeed this approximates to the average shape that has been calculated for odd dimers [53]. However, when the averages of properties such as the quadrupolar splittings are considered then it is

necessary to calculate the averaged shape in the frame relevant to that property, in other words, in the frame where the property does not change with the molecular conformation. For the deuterons localized in the terminal positions of the spacer in CB7CB-d_4 the natural frame would be with the major axis parallel to the para-axis of the cyanobiphenyl group. The conformational average would leave one cyanobiphenyl group of CB7CB unchanged but the averaged spacer and second mesogenic group should result in a uniaxial object parallel to the first mesogenic group containing the reference frame [54,55]. The order parameter for the para-axis with respect to the magnetic field, S_p, can be determined from the quadrupolar splittings of the prochiral deuterons via

$$S_p(T) = (2/3)|\Delta\nu(T)|q_{\mathrm{CD}}P_2(\cos\gamma), \tag{18}$$

where γ is the angle between a C-D bond and the para-axis. This is taken to be the tetrahedral angle 109.47° and the quadrupolar coupling constant, q_{CD}, is set equal to 168 kHz. The model gives the order parameter, $|S_p(T)|$, with respect to the helix axis as

$$|S_p(T)| = \left|S_p^n(T)P_2[\cos\theta_0(T)]\right|, \tag{19}$$

where S_p^n is also that for the para-axis but with respect to the director. The model of Jokisaari *et al.* [45] assumes specific temperature dependences for S_p^n and θ_0 which allow Eq. (19) to be written as

$$|S_p(T)| = |(1 - yT/T_{N_{\mathrm{TB}}N})^z P_2\{\cos[\theta(0)(1 - y_\theta T/T_{N_{\mathrm{TB}}N})^\beta]\}|, \tag{20}$$

where y and z are fitting parameters and y allows for the order parameter to be nonzero at the phase transition. Similarly $\theta(0)$, y_θ, and β are fitting parameters for the conical angle; $\theta(0)$ is that at absolute zero; and y_θ allows for the conical angle to be nonzero at the transition. Thus, in principle, this model can yield values for the order parameter of the mesogen in the N_{TB} phase as well as the conical angle from measurements of the mean splitting as a function of temperature.

The determination of the five parameters of the model from a limited data set presents a challenge. To simplify this a little we note that the mean splitting is almost continuous at the nematic to twist-bend nematic transition, and accordingly we assume that the conical angle is zero at the transition and the parameter y_θ is set equal to unity. However, y is not equal to 1 because the orientational order parameter, S_p^n, does not vanish at the transition. With these constraints, and within the experimental accuracy of the chiral splittings, we have fitted our measurements to the model using a least squares procedure [45]. The order parameters calculated in this way from the mean quadrupolar splittings, via Eq. (18), are shown as a function of the reduced temperature in Fig. 17(a). From the fitting, we have obtained the following values for the parameters of the model proposed by Jokisaari *et al.* [45]: $y = 0.919, z = 0.223, \theta(0) = 42.5°$, and $\beta = 0.374$. From the limited data set available, it is not possible to determine the uncertainties associated with these derived parameters, but these values allow us to calculate the order parameter for the para-axis of the cyanobiphenyl group and the conical angle in the twist-bend nematic phase.

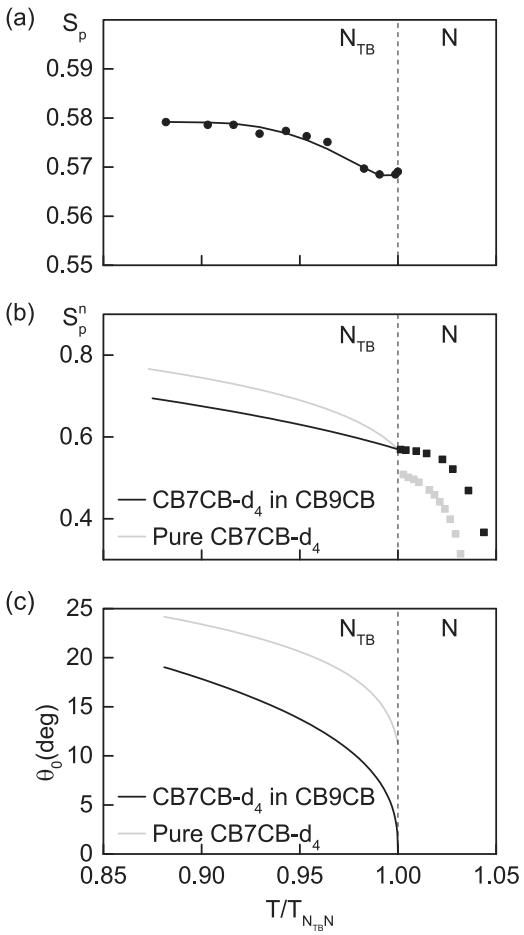

FIG. 17. (a) The dependence of the order parameter, S_p, on the reduced temperature in the twist-bend nematic phase, both experimental (•) and calculated (—). (b) The dependence of the orientational order parameter for the para-axis of the cyanobiphenyl group, S_p^n, for CB7CB-d_4 in CB9CB on the reduced temperature in the twist-bend nematic (indirect —) and nematic (direct ■) together with comparable results for pure CB7CB-d_4 (indirect —) and nematic (direct ■) [45]. (c) The dependence of the conical angle, θ_0, in the twist-bend nematic phase on the reduced temperature for CB7CB-d_4 in CB9CB (—) and for pure CB7CB-d_4 (—) [45].

Our results for the order parameters S_p^n in the N_{TB} phase as a function of the reduced temperature, $T/T_{N_{\mathrm{TB}}N}$, are shown as solid lines in Fig. 17(b).There appears to be a more or less linear increase in the order parameter with decreasing temperature. For comparison we also show results obtained in the same way for pure CB7CB-d_4 [45]. In addition we show in Fig. 17(b) the order parameters determined directly from the quadrupolar splittings in the nematic phase. The order parameter in the nematic phase is greater for CB9CB than for pure CB7CB. This difference is likely to result from the greater anisotropy or smaller curvature of CB9CB caused by its longer spacer. The other clear difference in behavior between the two dimers is the gradient in the order parameters prior to the N_{TB}-N transition; for CB9CB this is shallow but steeper for CB7CB. The most striking feature is the difference in the order parameters between the two nematic phases. Thus for CB9CB the order parameter is continuous, to within experimental error,

at the transition, but for CB7CB there is a strong jump in the order parameter at the N_{TB}-N transition showing a clear difference to the behavior of CB9CB. The Landau-like theory of Dozov [12] and the molecular theory of Greco *et al.* [26] both predict that the transition should be continuous.

We conclude with our results for the conical angle which is one of the defining characteristics of the twist-bend nematic phase. The values found for CB9CB are shown as a function of the reduced temperature in Fig. 17(c). Our experimental results for the mean splitting of the probe CB7CB-d_4 in CB9CB suggest that the N_{TB}-N transition is essentially continuous, and the conical angle is zero at the transition. In Fig. 17(c) we compare these results with those found for pure CB7CB using the same methodology [45]. It is clear that the dimer CB7CB appears to have a larger conical angle than its longer homologue CB9CB, which may be due to differences in the nature of the N_{TB}-N transition for the two dimers. The conical angles obtained from ^{2}H NMR mean splittings seem to be smaller than those estimated using other techniques, and so it may be useful to explore the use of different spin probes in the NMR experiments.

IV. CONCLUDING REMARKS

In summary, we have presented dielectric, calorimetric, and ^{2}H NMR studies on CB9CB. As expected, the properties of this odd liquid crystal dimer are similar to those of its shorter analogue CB7CB, but a more detailed analysis of the results provides more evidence concerning the structure of the twist-bend nematic phase for these cyanobiphenyl dimers with odd spacers. We have also shown that for CB9CB, high enough cooling rates prevent its crystallization and the N_{TB} mesophase becomes a twist-bend nematic glassy state.

The parallel component of the static dielectric permittivity reflects the phase transitions and shows a continuous decrease on cooling after entering the nematic phase which reflects the temperature dependence of the conformational distribution. This decrease leads to a decrease of the dielectric anisotropy which changes sign from positive to negative in the N_{TB} phase. The tilt of the director in the heliconical phase also plays a role in the sign change of the dielectric anisotropy. The appearance of tilt at the N-N_{TB} phase transition is clearly visible in dielectric experiments, similar to what was reported for CB7CB [2]. The contribution of the low-frequency mode to the perpendicular component of the permittivity shows an abrupt increase that can be explained by the rapid development of a director tilt of the average axis of the longitudinal dipole moment associated with the director.

The elastic constants K_1 and K_3 in the high temperature nematic phase of CB9CB show a behavior that is similar to that for other bent-shaped compounds: The splay elastic constant is larger than the bend elastic constant, and the latter decreases with decreasing temperature towards almost zero on approaching the N_{TB} phase. There is, however, a small increase in K_3 just prior to the formation of the N_{TB} phase as found for other odd dimers. Finally heat-capacity data measurements have allowed us to characterize the N_{TB}-N phase transition as first order, although nearly tricritical.

Our results confirm that the mesogenic dimer CB9CB forms a twist-bend nematic phase, as do other members of the homologous series. The properties of the N_{TB} phase of CB9CB are similar to those measured for its shorter homologue CB7CB, though the nature of the phase transition from nematic to twist-bend nematic appears to differ for the two homologues. Calorimetric measurements confirm that this transition in both materials is first order, though it is much closer to second order for the longer homologue CB9CB. ^{2}H NMR results also point to the weaker first-order character of the N_{TB}-N phase transition for CB9CB compared with CB7CB; for example, the chiral splitting for CB9CB, which provides clear evidence for the assignment of the N_{TB} phase, is almost continuous through the transition whereas for CB7CB this has a clear discontinuity. The analysis of the mean quadrupolar splitting allows the orientational order and conical angle to be estimated approximately throughout the N_{TB} phase; these contrast with the behavior of CB7CB which has a larger order and tilt angle than for CB9CB.

The results presented in this paper and other referenced work show that the introduction of core flexibility into mesogens can have a dramatic effect on both the properties and phase behavior of the materials. The appearance of a second nematic phase is perhaps the most dramatic consequence of the odd parity of the spacer combined with its flexibility in the cyanobiphenyl alkane dimers, but what is also remarkable is that the properties and nature of the phase transitions are critically dependent on the length of the methylene spacer, and by implication on the details of the chain flexibility. This adds a new dimension to the exploration of structure-property relationships for liquid crystal materials, and shows that in addition to their averaged bent shape and functionality the internal flexibility of mesogens is an important factor in determining their intriguing liquid crystal behavior.

ACKNOWLEDGMENTS

The authors are grateful for financial support from the MICINN project MAT2012-38538-C03-02,03 and from the Eusko Jaurlaritza-Gobierno Vasco (GI/IT-449-10). The authors also acknowledge the recognition from the Generalitat de Catalunya of GRPFM as Emergent Research Group (2009-SGR-1243). N.S. thanks the Alexander von Humboldt Foundation for a Postdoctoral Research Fellowship.

[1] V. P. Panov, M. Nagaraj, J. K. Vij, Y. P. Panarin, A. Kohlmeier, M. G. Tamba, R. A. Lewis, and G. H. Mehl, Phys. Rev. Lett. **105**, 167801 (2010).

[2] M. Cestari, S. Diez-Berart, D. A. Dunmur, A. Ferrarini, M. R. de la Fuente, D. J. B. Jackson, D. O. López, G. R. Luckhurst, M. A. Pérez-Jubindo, R. M. Richardson, J. Salud, B. A. Timimi, and H. Zimmermann, Phys. Rev. E **84**, 031704 (2011).

[3] P. A. Henderson and C. T. Imrie, Liq. Cryst. **38**, 1407 (2011).

[4] C. S. P. Tripathi, P. Losada-Pérez, C. Glorieux, A. Kohlmeier, M. G. Tamba, G. H. Mehl, and J. Leys, Phys. Rev. E **84**, 041707 (2011).

[5] M. Sepelj, A. Lesac, S. Baumeister, S. Diele, H. L. Nguyen, and D. W. Bruce, J. Mater. Chem. **17**, 1154 (2007).

[6] R. Balachandran, V. P. Panov, J. K. Vij, A. Kocot, M. G. Tamba, A Kohlmeier, and G. H. Mehl, Liq. Cryst. **40**, 681 (2013).

[7] V. Borshch, Y.-K. Kim, J. Xiang, M. Gao, A. Jákli, V. P. Panov, J. K. Vij, C. T. Imrie, M. G. Tamba, G. H. Mehl, and O. D. Lavrentovich, Nat. Commun. **4**, 2635 (2013).

[8] D. O. López, N. Sebastián, M. R. de la Fuente, J. C. Martínez-García, J. Salud, M. A. Pérez-Jubindo, S. Diez-Berart, D. A. Dunmur, and G. R. Luckhurst, J. Chem. Phys. **137**, 034502 (2012).

[9] K. Adlem, M. Čopič, G. R. Luchkurst, A. Mertelj, O. Parri, R. M. Richardson, B. D. Snow, B. A. Timimi, R. P. Tuffin, and D. Wilkes, Phys. Rev. E **88**, 022503 (2013).

[10] K. L. Atkinson, S. M. Morris, F. Castles, M. M. Qasim, D. J. Gardiner, and H. J. Coles, Phys. Rev. E **85**, 012701 (2012).

[11] M. Cestari, E. Frezza, A. Ferrarini, and G. R. Luckhurst, J. Mater. Chem. **21**, 12303 (2011).

[12] I. Dozov, Europhys. Lett. **56**, 247 (2001).

[13] P. J. Barnes, A. G. Douglass, S. K. Heeks, and G. R. Luckhurst, Liq. Cryst. **13**, 603 (1993).

[14] S. M. Shamid, S. Dhakal, and J. V. Selinger, Phys. Rev. E **87**, 052503 (2013). It should be mentioned that recently a distinction has been made between the bare bend elastic constant K_3 and the renormalized coefficient $K_{\rm eff}^3$ arising from Landau expansion, with the bare K_3 being always positive and $K_{\rm eff}^3$ the negative constant examined by Dozov.

[15] N. Sebastián, D. O. López, B. Robles-Hernández, M. R. de la Fuente, J. Salud, M. A. Pérez-Jubindo, D. A. Dunmur, G. R. Luckhurst, and D. J. B. Jackson, Phys. Chem. Chem. Phys. **16**, 21391 (2014).

[16] R. J. Mandle, E. J. Davis, C. T. Archbold, S. J. Cowling, and J. W. Goodby, J. Mater. Chem. C **2**, 556 (2014).

[17] P. K. Challa, V. Borshch, O. Parri, C. T. Imrie, S. N. Sprunt, J. T. Gleeson, O. D. Lavrentovich, and A. Jákli, Phys. Rev. E **89**, 060501 (R) (2014).

[18] L. Beguin, J. W. Emsley, M. Lelli, A. Lesage, G. R. Luckhurst, B. A. Timimi, and H. Zimmermann, J. Phys. Chem. B **116**, 7940 (2012).

[19] J. W. Emsley, M. Lelli, A. Lesage, and G. R. Luckhurst, J. Phys. Chem. B **117**, 6547 (2013).

[20] J. W. Emsley, P. Lesot, G. R. Luckhurst, A. Meddour, and D. Merlet, Phys. Rev. E **87**, 040501 (R) (2013).

[21] C. Greco, G. R. Luckhurst, and A. Ferrarini, Phys. Chem. Chem. Phys. **15**, 14961 (2013).

[22] D. Chen, J. H. Porada, J. B. Hooper, A. Klittnick, Y. Shen, M. R. Tuchband, E. Korblova, D. Bedrov, D. M. Walba, M. A. Glaser, J. E. Maclennan, and N. A. Clark, Proc. Natl. Acad. Sci. USA **110**, 15931 (2013).

[23] V. P. Panov, R. Balachandran, M. Nagaraj, J. K. Vij, M. G. Tamba, and A. Kohlmeier, Appl. Phys. Lett. **99**, 261903 (2011).

[24] V. P. Panov, R. Balachandran, J. K. Vij, M. G. Tamba, A. Kohlmeier, and G. H. Mehl, Appl. Phys. Lett. **101**, 234106 (2012).

[25] C. Meyer, G. R. Luckhurst, and I. Dozov, Phys. Rev. Lett. **111**, 067801 (2013).

[26] C. Greco, G. R. Luckhurst, and A. Ferrarini, Soft Matter **10**, 9318 (2014).

[27] A. G. Hoffmann, A.Vanakaras, A. Kohlmeier, G. H. Mehl, and D. J. Photinos. Soft Matter **11**, 850 (2015).

[28] M. Cifelli, S. V. Dvinskikh, and G. R. Luckhurst, presented at 25th International Liquid Crystal Conference, ILCC 2014, Dublin (unpublished).

[29] M. B. Sied, J. Salud, D. O. López, M. Barrio, and J. Ll. Tamarit, Phys. Chem. Chem. Phys. **4**, 2587 (2002).

[30] M. A. Anisimov, *Critical Phenomena in Liquids and Liquid Crystals* (Gordon and Breach Science Publishers, Amsterdam, 1991), and references therein.

[31] P. H. Keyes and J. R. Shane, Phys. Rev. Lett. **42**, 722 (1979).

[32] P. Cusmin, M. R. de la Fuente, J. Salud, M. A. Pérez-Jubindo, S. Diez-Berart, and D. O. López, J. Phys. Chem. B **111**, 8974 (2007).

[33] J. Salud, P. Cusmin, M. R. de la Fuente, M. A. Pérez-Jubindo, D. O. López, and S. Diez-Berart, J. Phys. Chem. B **113**, 15967 (2009).

[34] G. S. Iannacchione and D. Finotello, Phys. Rev. E **50**, 4780 (1994).

[35] S. Diez, D. O. López, M. R. de la Fuente, M. A. Pérez-Jubindo, J. Salud, and J. Ll. Tamarit, J. Phys. Chem. B **109**, 23209 (2005).

[36] E. G. Virga, Phys. Rev. E **89**, 052502 (2014).

[37] C. Meyer, G. R. Luckhurst, and I. Dozov, J. Mater. Chem. C **3**, 318 (2015).

[38] E. I. Kats and V. V. Levedev, JETP Lett. **100**, 110 (2014).

[39] A. Ferrarini, G. R. Luckhurst, P. L. Nordio, and S. J. Roskilly, Chem. Phys. Lett. **214**, 409 (1993).

[40] A. Ferrarini, G. R. Luckhurst, P. L. Nordio, and S. J. Roskilly, Liq. Cryst. **21**, 373 (1996).

[41] M. Stocchero, A. Ferrarini, G. J. Moro, D. A. Dunmur, and G. R. Luckhurst, J. Chem. Phys. **121**, 8079 (2004).

[42] D. A. Dunmur, G. R. Luckhurst, M. R. de la Fuente, S. Diez, and M. A. Peréz-Jubindo, J. Chem. Phys. **115**, 8681 (2001).

[43] N. Sebastián, M. R. de la Fuente, D. O. López, M. A. Pérez-Jubindo, J. Salud, and M. B. Ros, J. Phys. Chem. B **117**, 14486 (2013).

[44] N. Sebastián, M. R. de la Fuente, D. O. López, M. A. Pérez-Jubindo, J. Salud, S. Diez-Berart, and M. B. Ros, J. Phys. Chem. B **115**, 9766 (2011).

[45] J. P. Jokisaari, G. R. Luckhurst, B. A. Timimi, J. Zhu, and H. Zimmermann, Liq. Cryst. **42**, 708 (2015).

[46] C. J. Yun, M. R. Vengatesan, J. K. Vij, and J. K. Song, Appl. Phys. Lett. **106**, 173102 (2015).

[47] S. W. Morris, P. Palffy-Muhoray, and D. A. Balzarini, Mol. Cryst. Liq. Cryst. **139**, 263 (1986).

[48] M. G. Clark, E. P. Raynes, R. A. Smith, and R. J. A. Tough, J. Phys. D: Appl. Phys. **13**, 2151 (1980).

[49] N. Sebastián, B. Robles-Hernández, D. O. López, M. R. de la Fuente, S. Diez-Berart, J. Salud, D. Dunmur, and G. R. Luckhurst, presented at 25th International Liquid Crystal Conference, ILCC 2014, Dublin (unpublished).

[50] B. Kundu, R. Pratibha, and N. V. Madhusudana, Phys. Rev. Lett. **99**, 247802 (2007).

[51] P. Sathyanarayana, V. S. R. Jampani, M. Skarabot, I. Musevic, K. V. Le, H. Takezoe, and S. Dhara, Phys. Rev. E **85**, 011702 (2012).

[52] C. T. Imrie and G. R. Luckhurst, in *Handbook of Liquid Crystals*, edited by J. W. Goodby, P. J. Collings, T. Kato, C. Tschierske, H. F. Gleeson, and P. Raynes (Wiley-VCH, Weinheim, 2014), Vol. 7, Part II.

[53] G. R. Luckhurst, Macromol. Symp. **96**, 1 (1995).

[54] A. Kloczkowski, G.R. Luckhurst, and R.W. Phippen, Liq. Cryst. **3**, 185 (1998).

[55] A. Emerson, G.R. Luckhurst, and R.W. Phippen, Liq. Cryst. **10**, 1 (1991).